Effect of Cr substitution on the electronic structure of $CuAl_{1-x}Cr_xO_2$

David O. Scanlon, Aron Walsh,* Benjamin J. Morgan, and Graeme W. Watson†
School of Chemistry, Trinity College Dublin, Dublin 2, Ireland

David J. Payne and Russell G. Egdell
Department of Chemistry, Inorganic Chemistry Laboratory, Oxford University, South Park Road, Oxford OX1 3QR, United Kingdom
(Received 18 September 2008; published 5 January 2009)

The geometries and electronic structures of $CuAl_{1-x}Cr_xO_2$ have been investigated using density-functional theory with on-site corrections for strongly correlated systems (GGA+U) for $x=0,\frac{1}{2},1$. Al is found to be well described within the ionic model, with a valence charge corresponding to a +3 oxidation state. Substituting Cr for Al is predicted to increase the density of states at the top of the valence band, in agreement with experimental x-ray photoemission spectroscopy data. Analysis of atom-projected densities of states and valence charges suggests that this is due to increased covalency between Cr and O; the valence charge for O in the Cu-O-(Al,Cr) subunits changes from −1.74 to ~−1.25 when Cr replaces Al. This produces an indirect oxygen-mediated change to the Cu d states.

DOI: 10.1103/PhysRevB.79.035101 PACS number(s): 71.20.−b, 72.80.Ga, 71.15.Mb

I. INTRODUCTION

The coexistence of electrical conductivity and optical transparency in a single material was first observed for cadmium oxide films in the 1950s.[1] This combination of technologically useful properties has numerous potential applications, including solar cells, flat panel displays, electromagnetic shielding devices, light-emitting diodes, and transparent heat sources.[2] It is hoped that such transparent conducting oxides (TCOs) may be used in the fabrication of functional p-n junctions, making possible a variety of transparent electronic devices. To prevent adsorption of visible photons TCO materials should have an optical band gap greater than 3 eV and to ensure concomitant conductivity should possess carrier concentrations of at least 10^{20} cm^{-3}.

In contrast with archetypal TCOs such as ZnO, In_2O_3, and SnO_2, which are intrinsically n-type,[3] p-type TCOs have proved more elusive. In wide-band-gap oxides the top of the valence band is predominately composed of O $2p$ states. Traditional p-type doping approaches fail, as holes introduced to the valence-band edge are trapped on oxygen atoms and cannot migrate.[4] Effective transport of positive holes requires disperse electronic states at the top of the valence band. Suitable covalent states can be generated by coupling the electronic states of oxygen with those of metals that possess closed-shell valence electronic configurations, typically those with complete low-binding-energy d shells, such as Cu and Ag.[5]

One of the first reported p-type TCOs was $CuAlO_2$, which adopts the delafossite mineral structure ($CuFeO_2$).[6] In this structure each Cu atom is linearly coordinated between two oxygen atoms, forming O-Cu-O dumbbells parallel to the c axis (Fig. 1). Oxygens in these O-Cu-O units are also coordinated to three Al atoms, oriented such that Al-centered octahedra form AlO_2 layers which lie parallel to the ab plane. Two alternative layer stackings are possible, resulting in a hexagonal (space group $P63/mmc$) or rhombohedral (space group $R3$-mh) unit cell.[7] An optical band gap of 3.5 eV ensures transparency in the visible region.[8]

When Al is replaced with other metals—e.g., Ga, In, and Sn—the delafossite structure and wide band gap are maintained and such doped materials have been the subject of experimental interest.[9] Bipolar doping of $CuInO_2$ has been achieved with Ca (p-type) and Sn (n-type) dopants.[10,11] $CuCrO_2$, with an optical band gap of ~3.08 eV, has recently been the focus of interest as a p-type TCO,[12] with Mg-doped $CuCrO_2$ having the highest reported p-type conduction of any delafossite-structured TCO.[13] Studies are now focusing on improving the conductivity of $CuCrO_2$ by doping with other divalent dopants, such as Ni (Ref. 14) and Cd.[15]

Numerous computational and theoretical studies of p-type TCO materials have been published, but in the case of $CuAlO_2$ these have tended to neglect the underlying chemistry in favor of analyses of the effects of doping on the band structure.[16–20] In $CuAlO_2$, the effects of Cu and Al vacancies, and Be, Mg, and Ca dopants, have been investigated using local-density approximation (LDA)-based linearized augmented-plane-wave (LAPW) calculations.[16] This study suggested that the most promising defects for improving p-type conductivity are Cu vacancies and Be doping at Al sites. Nie *et al.*[19] also employed LDA within the LAPW method to investigate bipolar doping and band-gap anomalies in delafossite TCOs. The calculated band structures for $CuAlO_2$, $CuGaO_2$, and $CuInO_2$ show an indirect fundamental band gap, in agreement with band structures for the hexagonal $CuAlO_2$ structure calculated by Robertson *et al.*[18] Layer stacking has little effect on the minimum gap, with an indi-

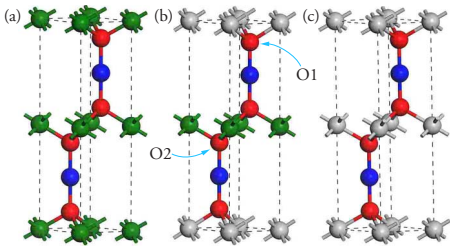

FIG. 1. (Color online) The crystal structures of (a) $CuAlO_2$, (b) $CuAl_{0.5}Cr_{0.5}O_2$, and (c) $CuCrO_2$. Red atoms are O, blue Cu, green Al, and gray Cr. The two O sites that are inequivalent in $CuAl_{0.5}Cr_{0.5}O_2$ are labeled in the middle panel.

 ©2009 The American Physical Society

TABLE I. Structural data for the DFT-GGA+U optimized $CuAl_{1-x}Cr_xO_2$ ($x=0,\frac{1}{2},1$) structures and percentage error with respect to experimental data (Refs. 7 and 29). Lattice dimensions are given in Å and volumes in Å^3.

	$CuAlO_2$	$CuAl_{0.5}Cr_{0.5}O_2$	$CuCrO_2$
Volume	81.79	86.95	92.50
a	2.885(+0.7%)	2.965	3.055(+2.9%)
c	11.340(+0.2%)	11.418	11.416(+0.1%)

rect gap of 2.1 eV predicted for both the hexagonal and rhombohedral sequences. An LDA study of native defects in $CuAlO_2$ was also carried out by Hamada and Katayama-Yoshida,[20] which concluded that Cu vacancies and O interstitials are the relevant defects and that control of the copper and oxygen partial pressures is essential for the fabrication of low-resistivity $CuAlO_2$.

II. THEORETICAL METHODS

Here we report calculations on the electronic structure of $CuAl_{1-x}Cr_xO_2$ for $x=0,\frac{1}{2},1$. All calculations were performed using the periodic density-functional theory (DFT) code VASP,[21] in which valence electronic states are expanded as a set of plane waves, and core electrons are described through the projector augmented wave approach,[22] with cores of [Ar] for Cu, [Ar] for Cr, [Ne] for Al, and [He] for O. The Perdew-Burke-Ernzerhof[23] gradient corrected functional was used with corrections for on-site Coulomb interactions for strongly correlated systems [generalized gradient approximation (GGA)+U].[24] GGA typically underbinds localized orbitals such as metal d states and the +U modification provides an approximate correction for this shortcoming.[25] The values of U employed were 5.2 eV for the Cu d states, which closely reproduces features of the experimental x-ray photoemission spectroscopy (XPS) for Cu_2O, and is close to the effective U value of 5 eV used for Cu_2O by Raebiger *et al.*;[26] and 4 eV for the Cr d states, which reproduces the valence-band features of Cr_2O_3.[27] All calculations were performed on eight atom hexagonal unit cells, using a $9\times9\times5$ Monkhorst-Pack k-point mesh and a 500 eV plane-wave cutoff. The calculations on both systems containing open-d-shell Cr atoms were spin polarized. Geometric relaxations were performed, which were deemed to be converged when the forces on all the atoms were less than 0.001 eV Å^{-1}.

III. RESULTS

Structural optimizations at a series of volumes were performed for $CuAl_xCr_{1-x}O_2$ ($x=0,\frac{1}{2},1$), allowing the atomic positions and lattice vectors and angles to relax within a constrained total volume. The equilibrium cell volume was obtained by fitting the resulting energy-volume curve to the Murnaghan equation of state.[28] The cell parameters thus obtained are listed in Table I, and the resulting structures are plotted in Fig. 1. The optimized lattice vectors are overestimated as is expected with GGA, yet remain within 2.9% of experimental values.[7,29]

TABLE II. Nearest-neighbor interatomic distances (in Å) for $CuAlO_2$, $CuAl_{0.5}Cr_{0.5}O_2$, and $CuCrO_2$.

	$CuAlO_2$	$CuAl_{0.5}Cr_{0.5}O_2$	$CuCrO_2$
Cu-O (Al)	1.866	1.865	
Cu-O (Cr)		1.846	1.844
Al-O	1.928	1.958	
Cr-O		2.008	2.032

A. $CuAlO_2$

Table II lists the nearest-neighbor interatomic distances for the optimized structures. In $CuAlO_2$ the Cu ions are linearly coordinated to two equidistant oxygen atoms at 1.866 Å. The Al-O distances in the Al-centered coordination octahedra are 1.928 Å. These bond lengths are in excellent agreement with experiment.[7,29] The calculated band structure is shown in Fig. 2. The conduction-band minimum (CBM) is at Γ and a broad valence-band maximum (VBM) is found along H-K, and extending past K along the K-Γ direction, in good agreement with previous calculations.[18,30] Robertson *et al.*[18] previously predicted the VBM to be at L, and the highest-occupied band at this k vector for the band structure presented here is only 0.1 eV below the VBM. The band gap is indirect and measures 2.2 eV. This is overestimated compared to the value of 1.8 eV obtained from optical-absorption experiments,[8] although it has been proposed that intrinsic defect levels in experimental samples decrease this experimental value.[18] The smallest direct band gap is at Γ and measures 3.1 eV, compared to the experimental value of 3.5 eV.[8]

The calculated total and partial (ion decomposed) electronic densities of states (EDOS/PEDOS) for $CuAlO_2$ are shown in Fig. 3. The PEDOS were calculated by projecting the wave functions onto atom centered spherical harmonics, using radii of 1.4 Å for Cu, 1.2 Å for Al, and 1.4 Å for O. The ratios are consistent with the positions of minima observed in valence-charge-density plots and result in the cor-

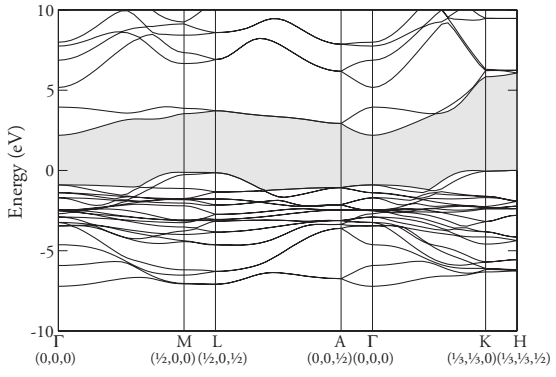

FIG. 2. The electronic band structure of $CuAlO_2$ along the high-symmetry points, plotted with reference to the top of the valence band at 0 eV. The valence-band–conduction-band gap is shaded.

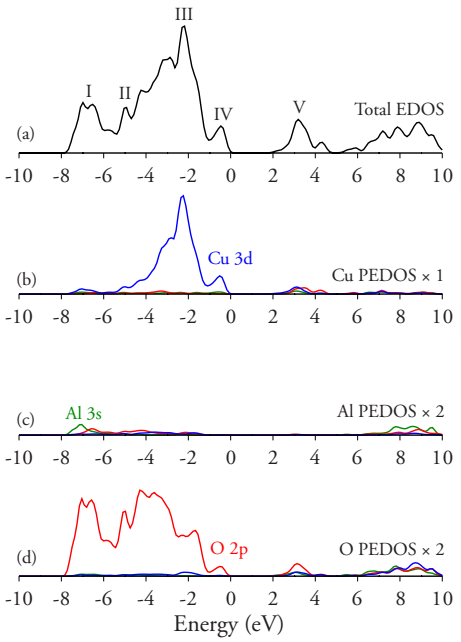

FIG. 3. (Color online) The electronic density of states for $CuAlO_2$. (*a*) Total EDOS, (*b*) Cu PEDOS, (*c*) Al PEDOS ×2 and (*d*) O PEDOS ×2. The blue lines represent *d* states, green *s* states, and red *p* states.

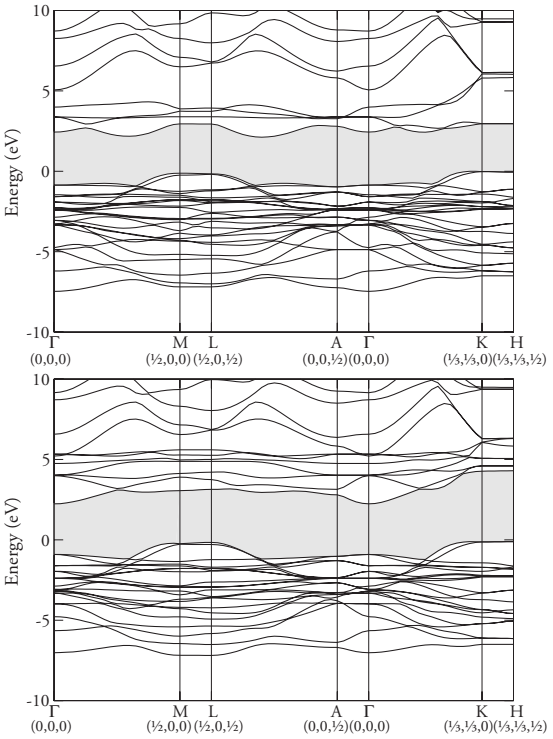

FIG. 4. The electronic band structure of $CuAl_{0.5}Cr_{0.5}O_2$ along the high-symmetry points, plotted with reference to the top of the valence band at 0 eV. The valence-band–conduction-band gap is shaded. The upper panel shows the α-spin bands and the lower the β-spin bands.

rect number of total electrons in each system. Four peaks are distinguishable in the valence band at −7, −5, −3, and −1 eV (labeled I–IV), which is consistent with recent XPS measurements reported by Aston *et al.*[31] The conduction band displays a narrow peak between +2 and +4 eV, labeled V, with a second broad peak above 6 eV.

The Cu PEDOS is dominated by 3*d* states between −4 and −1 eV, corresponding to peaks III and IV in the EDOS. There are also Cu 3*d* states between −8 and −4 eV, indicating a degree of covalent bonding with oxygen. The Al PEDOS shows a very small valence-band contribution concentrated between −8 and −4 eV which consists mainly of 3*s* and 3*d* states. The observed contribution is mainly due to the overlap of the projected spherical harmonics with charge on neighboring O atoms and is not significant. In the conduction band the onset of Al states does not occur until +5 eV. The Al contributions to the EDOS are small, as is expected for an atom which is often well described by a fully ionized +3 oxidation state, and Al makes an insignificant contribution to the states determining the electronic conduction properties. The O PEDOS displays all five peaks observed in the EDOS. Peak I is O 2*p* in nature, with peak II also mainly O 2*p*, although with additional Cu 3*d* states present. Peak III is mostly Cu 3*d* with some O 2*p* contribution, while peak IV contains a mixture of O 2*p* and Cu 3*d* states. The bottom of the conduction band and top of the valence band both consist of states derived from a mixture of Cu 3*d* and O 2*p*.

B. $CuAl_{0.5}Cr_{0.5}O_2$

Introducing Cr into the Al lattice sites in alternating *ab* layers has a significant effect on the structure, as can be seen by considering bond lengths. As shown in Fig. 1(b), oxygen atoms now exist in two environments: O1 situated between Cu and Cr and O2 which is coordinated to Cu and Al. The bond lengths are given in Table II. The Cu-O1 bond length decreases to 1.85 Å, relative to the Cu-O distance in $CuAlO_2$ of 1.87 Å, whereas the Cu-O2 bond length is unchanged. The Al-O2 bond length is also unchanged from the $CuAlO_2$ value of 1.93 Å, indicating the local O coordination environment is only dependent on the identity of the directly bonded atoms. The Cr-O bond length is 2.01 Å.

The calculated band gap is indirect and measures 2.2 eV, unchanged from $CuAlO_2$. However, the band structure (Fig. 4) shows that the CBM is no longer at Γ but occurs along the line from *L* to *A*, with the VBM appearing just off *K* in the direction of Γ. Along the same *K*-Γ direction but closer to Γ, there is a direct band gap of 2.8 eV, and a second direct gap of 2.8 eV is found along *L*-*A* close to *L*.

The EDOS and PEDOS for $CuAl_{0.5}Cr_{0.5}O_2$ for both α- and β-spin components are shown in Fig. 5. The PEDOS were calculated using the same ionic radii as for $CuAlO_2$, with 1.2 Å used for the Cr radius. Five regions are noted and labeled I–V as for $CuAlO_2$. Region I makes up the bottom of the conduction band and is mostly O 2*p* in origin, with some contribution from Cr. The O1 PEDOS itself is spin polarized, in response to the direct contact with spin polarized Cr ions. On substitution at the Al site, Cr adopts a formal oxidation state of Cr(III) producing a $3d^3$ ion. The approximately octahedral crystal field removes the *d* orbital degeneracy and increases the energy of the e_g states. The favored electronic configuration is thus high spin t_{2g}^3. Peaks III and IV are

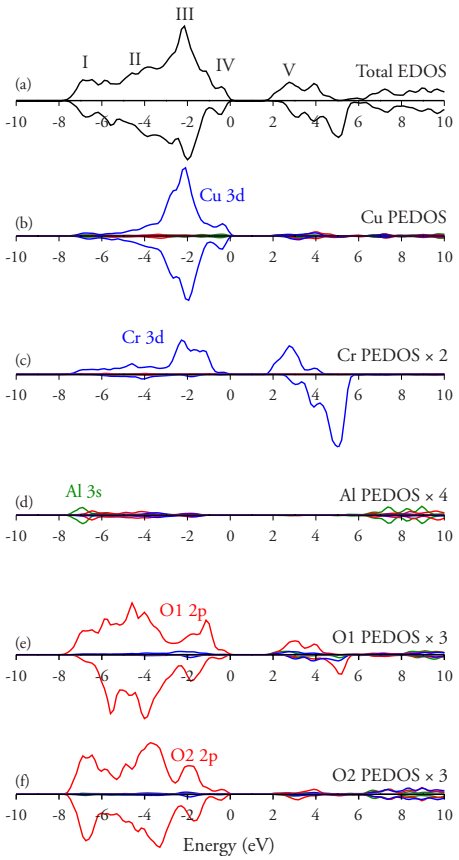

FIG. 5. (Color online) The electronic density of states for $CuAl_{0.5}Cr_{0.5}O_2$. (a) Total EDOS; (b) Cu PEDOS; (c) Cr PEDOS ×2; (d) Al PEDOS ×4; and [(e) and (f)] O PEDOS ×3. The blue lines represent *d* states, green *s* states, and red *p* states.

mainly Cu 3*d*, both with some Cr 3*d* and O 2*p* characters. The Cr contribution to IV increases the density of states at the top of the valence band, relative to that for $CuAlO_2$. The appearance of a small shoulder at −1 eV for the α-spin component is due to a change in the O1-Cu interaction, caused by the presence of the adjacent Cr. The bottom of the conduction band (V) is dominated by Cr states, with the onset of the Al states at 6 eV. Compared to $CuAlO_2$, oxygen contributes more strongly to the bottom of the conduction band—O1 in particular—indicating a significant O1-Cr interaction which is absent for O2-Al, which is likely to be responsible for the change in *k* vector of the VBM on doping from $CuAlO_2$ to $CuAl_{0.5}Cr_{0.5}O_2$.

C. $CuCrO_2$

The $CuCrO_2$ bond lengths are listed in Table II. The Cu-O distance is marginally changed at 1.84 Å and the Cr-O bond lengths have extended to 2.03 Å, which is consistent with diffraction data.[32] The band structure (Fig. 6) again exhibits an indirect band gap, here of 2.04 eV, while the direct gap measures 2.55 eV and is found near *M* along *M*-Γ. For $CuCrO_2$ there is an experimentally demonstrated redshift in the experimental optical absorption relative to $CuAlO_2$. As is the case for $CuAl_{0.5}Cr_{0.5}O_2$, the CBM is centered between *L* and *A* and the VBM is situated at *M*. The presence of two Cr

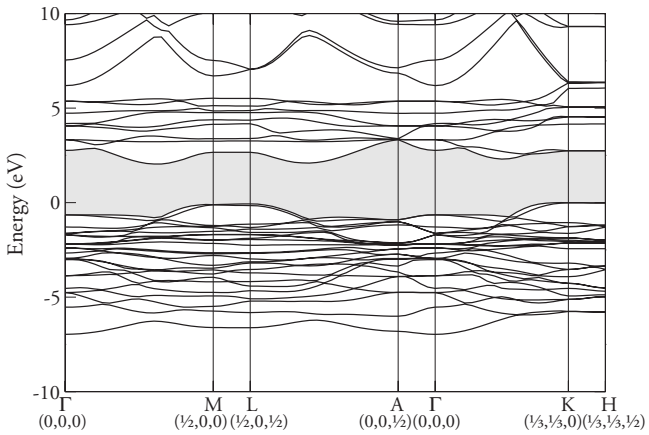

FIG. 6. The electronic band structure of $CuCrO_2$ along the high-symmetry points, plotted with reference to the top of the valence band at 0 eV.

sites introduces the possibility of magnetic ordering within the periodicity of the simulated unit cell. Due to the t_{2g}^3 configuration, antiferromagnetic (AF) interactions are stabilized, while ferromagnetic (FM) interactions result in no net energy gain. The calculated energy difference between the AF and FM configurations is small at 20 meV/f.u., consistent with the low Curie temperature reported in experiment.[33] The EDOS of $CuCrO_2$ (Fig. 7) is similar to that of $CuAl_{0.5}Cr_{0.5}O_2$. In $CuAl_{0.5}Cr_{0.5}O_2$, however, the Cr PEDOS displays two peaks at −2.5 and −1 eV of approximately equal height, whereas for $CuCrO_2$ the peak at ~−2.5 eV dominates. The Cu peak shape is also affected: the shoulder to the left of the maximum just below −2 eV is less pronounced and a second shoulder now appears to the high-energy side of the main peak. The bottom of the conduction band is predominantly Cr in nature, with the contribution

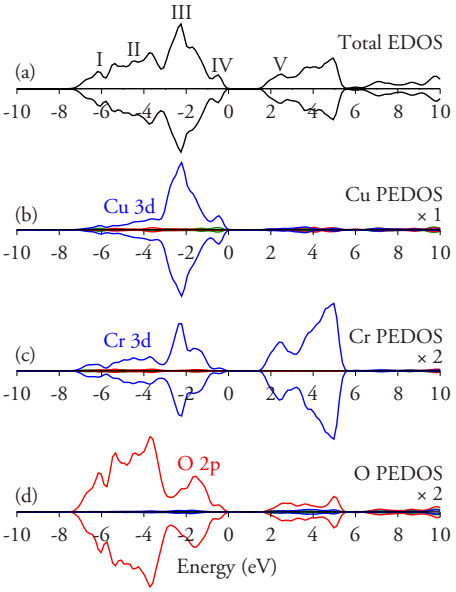

FIG. 7. (Color online) The electronic density of states for $CuCrO_2$. (a) Total EDOS, (b) Cu PEDOS, (c) Cr PEDOS ×2, and (d) O PEDOS ×2. The blue lines represent *d* states, green *s* states, and red *p* states.

TABLE III. Bader partial electron charges for $CuAlO_2$, $CuAl_{0.5}Cr_{0.5}O_2$, and $CuCrO_2$.

	$CuAlO_2$	$CuAl_{0.5}Cr_{0.5}O_2$	$CuCrO_2$
Cu	+0.49	+0.57	+0.58
Al	+3.00	+3.00	
Cr		+1.92	+1.93
O1	−1.74	−1.23	−1.25
O2	−1.74	−1.78	−1.25

from O $2p$ states now extending up to ~5 eV due to increased interaction with the Cr $3d$ states.

IV. DISCUSSION

Using Bader partial charge analysis, it is possible to quantify how the distribution of charge changes as Cr progressively replaces Al. Bader charges also give an indication of the applicability of an ionic description to the charge distribution. The calculated charges are listed in Table III. For $CuAlO_2$, this gives charges of +3e for Al, +0.49e for Cu, and −1.74e for O. Al is well described by a formal ion in a +3 oxidation state. The charges for Cu and O are less than those expected from purely ionic considerations, which agrees with the interpretation of the PEDOS that there is covalent mixing between Cu and O to form the valence-band states.

Charge analysis of $CuAl_{0.5}Cr_{0.5}O_2$ gives charges of +0.57e for the Cu, +3e for the Al, −1.23e for O1, −1.78e for O2, and 1.92e for Cr. Again Al is well described as fully ionic. Cu is slightly more ionic than in $CuAlO_2$, and O1 is significantly less ionic, while Cr is less ionic than the Al it replaces. This indicates partial charge transfer from O1 to Cr and a *reduced* amount of charge transfer from O1 to Cu and supports the interpretation of the PEDOS that Cr contributes significantly to the top of the valence band and bottom of the conduction band.

For $CuCrO_2$ charges of +0.58e for Cu, +1.93e for Cr, and −1.25e for O are found, indicating valence charge distributed between all three species. Both O are less ionic than in $CuAlO_2$, with charges close to that for O1 in $CuCrO_2$, as is expected since both Al sites have been occupied by Cr. The valence electron density supports an indirect Cr-Cu interaction, mediated through the oxygens with which Cr now is directly hybridized. This contribution of Cr to the band edges produces the flattening of the CBM seen in the band structure, due to the localized nature of the $3d$ states compared to the dispersive cation-s-derived CBM in $CuAlO_2$ (Fig. 6).

Figure 8 shows simulated spectra for $CuAlO_2$ and $CuCrO_2$. These have been constructed by performing weighted summations of the atom-projected densities of states. The coefficients used are the calculated scattering cross sections as given in Ref. 34. These simulated spectra can be compared directly to experimental XPS data of Cr doping in $CuAlO_2$ (Ref. 35) (Fig. 9). The lower panel of Fig. 8 ($CuAlO_2$) shows good agreement with the experimental line shape. In particular, the main peak at −3 eV displays a shoulder on the left which is also seen in the experimental

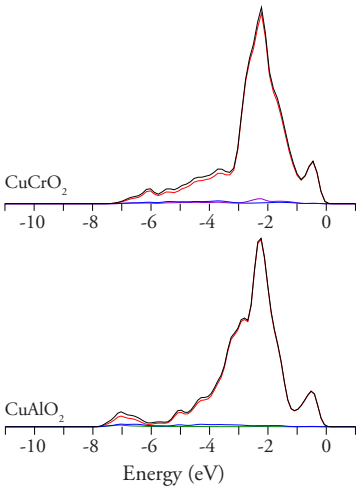

FIG. 8. (Color online) GGA+U cross-section weighted DOS for $CuCrO_2$ (top) and $CuAlO_2$ (bottom). In each case the black curve is the summed DOS. The atom specific components are shown as red (Cu), blue (O), violet (Cr), and green (Al).

XPS. For $CuCrO_2$ (upper panel of Fig. 8) the shoulder to the left of the main peak is smaller than in $CuAlO_2$ and a second shoulder is seen to the right. Again these features are observed in the experimental $CuCrO_2$ XPS. The large scattering cross section of Cu $3d$ states (1.20 kb) compared with Cr $3d$ states (0.18 kb) means this change in features is not due to a direct probing of Cr states produced on doping since these contribute minimally to the simulated spectra. Instead a change in the distribution of Cu states is observed, which is brought about by the presence of Cr, through an indirect interaction via the mutually bonded O atoms. This produces hybridized states at the top of the valence band, as seen above in the calculated DOSs (Figs. 3 and 7).

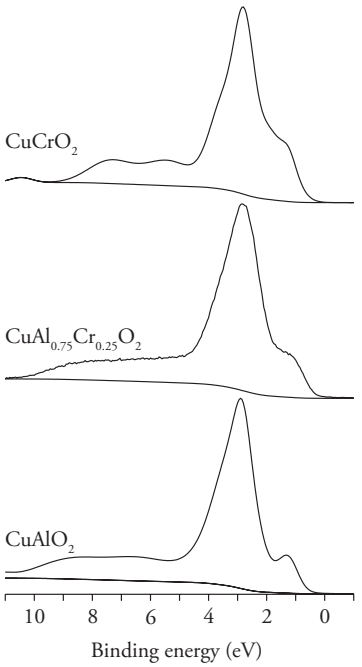

FIG. 9. Experimental XPS valence band of $CuCrO_2$ (top), $CuAl_{0.75}Cr_{0.75}O_2$ (middle), and $CuAlO_2$ (bottom) (Ref. 35).

In light of this it is constructive to examine the work of Nagarajan *et al.*[13] who compared the *p*-type conductivity of Mg-doped $CuCrO_2$, $CuScO_2$, and $CuYO_2$. They found decreasing conductivity across this series, which tracks an increase in the size of the M^{3+} ion and a consequent increase in the Cu-Cu distance. They therefore proposed that increased overlap between Cu *d* bands produces better charge mobility. The in-plane Cu-Cu distance, however, is clearly not the only factor determining conductivity on Mg doping since Mg-doped $CuAlO_2$ displays a lower conductivity than Mg-doped $CuCrO_2$,[13] despite the Cu-Cu distance being smaller in the Al based delafossite. Our results indicate that the occupied Cr 3*d* states interact covalently with the neighboring O atoms and hence indirectly modify the Cu 3*d* states, an effect which the $2p^6$ Al atoms are unable to produce. This increases the density of states at the top of the valence band, which are precisely those states expected to determine the mobility of *p*-type charge carriers formed on doping. It is therefore likely that chemical differences between Cr, Sc, and Y also play a role in determining the relative conductivities of these materials when doped to form *p*-type conductors.

V. CONCLUSION

The electronic structure and geometries of $CuAlO_2$, $CuAl_{0.5}Cr_{0.5}O_2$, and $CuCrO_2$ have been investigated using DFT+*U*, and calculated band structures and atom-decomposed densities of states have been presented. Replacing Al with Cr results in the appearance of Cr 3*d* states that are found throughout the majority of the valence band, with significant Cr-O interaction, which indirectly changes the Cu-O interaction. This causes an increase in the density of Cu 3*d* states at the top of the valence band, as seen in recent XPS studies.[35] Cr 3*d* states are also present at the bottom of the conduction band and the conduction-band minimum moving away from Γ as a result. The indirect nature of the band gap is maintained. Bader analysis highlights the ionic nature of Al in $CuAlO_2$ and shows significant covalency between Cr and O states in $CuAl_{0.5}Cr_{0.5}O_2$ and $CuCrO_2$.

ACKNOWLEDGMENTS

This publication has emanated from research conducted with financial support of Science Foundation Ireland under PI Grant No. 06/IN.1/I92. We also acknowledge support from the HEA for the PTRLI programs IITAC (cycle III) and E-INIS (cycle IV). All calculations were performed on the IITAC supercomputer as maintained by the Trinity Centre for High Performance Computing (TCHPC). Work on transparent conducting oxides in Oxford was supported under EPSRC-GB under Grant No. GR/S94148.

*Present address: National Renewable Energy Laboratory, Golden, CO 80401, USA.

†Author to whom correspondence should be addressed; wastong@tcd.ie

[1] G. Helwig, Z. Phys. **132**, 621 (1952).
[2] T. Minami, Semicond. Sci. Technol. **20**, S35 (2005).
[3] C. G. Granqvist and A. Hultaker, Thin Solid Films **411**, 1 (2002).
[4] S. Sheng, G. Fang, C. Li, S. Xu, and X. Zhao, Phys. Status Solidi A **203**, 1891 (2006).
[5] K. G. Godinho, G. W. Watson, A. Walsh, A. J. H. Green, D. J. Payne, J. Harmer, and R. G. Egdell, J. Mater. Chem. **18**, 2798 (2008).
[6] A. Trovarelli, C. de Leitenburg, M. Boaro, and G. Dolcetti, Catal. Today **50**, 353 (1999).
[7] B. U. Köhler and M. Jansen, Z. Anorg. Allg. Chem. **543**, 73 (1986).
[8] H. Yanagi, S.-I. Inoue, K. Ueda, H. Kawazoe, H. Hosono, and N. Hamada, J. Appl. Phys. **88**, 4159 (2000).
[9] K. Ueda, T. Hase, H. Yanagi, H. Kawazoe, H. Hosono, H. Ohta, M. Orita, and M. Hirano, J. Appl. Phys. **89**, 1790 (2001).
[10] H. Yanagi, T. Hase, S. Ibuki, K. Ueda, and H. Hosono, Appl. Phys. Lett. **78**, 1583 (2001).
[11] L. Liu, K. Bai, H. Gong, and P. Wu, Chem. Mater. **17**, 5529 (2005).
[12] S. Mahapatra and S. A. Shivashankar, Chem. Vap. Deposition **9**, 238 (2003).
[13] R. Nagarajan, A. D. Draeseke, A. W. Sleight, and J. Tate, J. Appl. Phys. **89**, 8022 (2001).
[14] S. Y. Zheng, G. S. Jiang, J. R. Su, and C. F. Zhan, Mater. Lett. **60**, 3871 (2006).
[15] M. V. Lalić and J. Mestnik-Filho, J. Phys.: Condens. Matter **18**, 1619 (2006).
[16] H. Katayama-Yoshida, T. Koyanagi, H. Funashima, H. Harima, and A. Yanase, Solid State Commun. **126**, 135 (2003).
[17] H. Kizaki, K. Sato, and H. Katayama-Yoshida, Jpn. J. Appl. Phys. **47**, 6488 (2008).
[18] J. Robertson, P. W. Peacock, M. D. Towler, and R. Needs, Thin Solid Films **411**, 96 (2002).
[19] Xiliang Nie, S.-H. Wei, and S. B. Zhang, Phys. Rev. Lett. **88**, 066405 (2002).
[20] I. Hamada and H. Katayama-Yoshida, Physica B **376-377**, 808 (2006).
[21] G. Kresse and J. Furthmüller, Phys. Rev. B **54**, 11169 (1996).
[22] G. Kresse and D. Joubert, Phys. Rev. B **59**, 1758 (1999).
[23] J. P. Perdew, K. Burke, and M. Ernzerhof, Phys. Rev. Lett. **77**, 3865 (1996).
[24] S. L. Dudarev, G. A. Botton, S. Y. Savrasov, C. J. Humphreys, and A. P. Sutton, Phys. Rev. B **57**, 1505 (1998).
[25] B. J. Morgan, D. O. Scanlon, and G. W. Watson, e-J. Surf. Sci. Nanotechnol. (to be published).
[26] H. Raebiger, S. Lany, and A. Zunger, Phys. Rev. B **76**, 045209 (2007).
[27] A. Rohrbach, J. Hafner, and G. Kresse, Phys. Rev. B **70**, 125426 (2004).
[28] F. D. Murnaghan, Proc. Natl. Acad. Sci. U.S.A. **30**, 244 (1944).
[29] O. Crottaz, F. Kubel, and H. Schmid, J. Solid State Chem. **122**, 247 (1996).

[30] X. L. Nie, S. H. Wei, and S. B. Zhang, Phys. Rev. B **65**, 075111 (2002).
[31] D. J. Aston, D. J. Payne, A. J. H. Green, R. G. Egdell, and D. S. L. Law, J. Guo, P.-A. Glans, T. Learmonth, and K. E. Smith, Phys. Rev. B **72**, 195115 (2005).
[32] O. Crottaz and F. Kubel, Z. Kristallogr. **211**, 481 (1996).
[33] T. Okuda, N. Jufuku, S. Hidaka, and N. Terada, Phys. Rev. B **72**, 144403 (2005).
[34] J. J. Yeh and I. Lindau, At. Data Nucl. Data Tables **32**, 1 (1985).
[35] T. Arnold *et al.* (unpublished).